Association of Dicyanodiphenylacetylenes with Silver(I) Salts in Solution and Solid State: Electrospray Ionization Mass Spectrometry Samples Aggregates at Subsaturated Concentrations

Keith A. Hirsch,† Scott R. Wilson,† and Jeffrey S. Moore*,‡

Contribution from the Departments of Chemistry and Materials Science and Engineering, The University of Illinois at Urbana-Champaign, 600 South Mathews Avenue, Urbana, Illinois 61801

Received April 9, 1997[⊗]

Abstract: Complexes of 2,3′-dicyanodiphenylacetylene (2,3′-DCPA, **1**), 2,2′-dicyanodiphenylacetylene (2,2′-DCPA, **2**), and 2,4′-dicyanodiphenylacetylene (2,4′-DCPA, **3**) with silver(I) salts have been characterized in the solid state by single-crystal X-ray analysis. In addition, aggregates of compounds **1**−**3** and silver(I) ions have been identified in solution by electrospray ionization mass spectrometry (ESI-MS). The topology of the structures in the solid state, namely finite versus infinite, is found to depend on the substitution pattern of nitrile groups on diphenylacetylene. For 2,3′-DCPA (**1**), crystallization with silver(I) triflate ($AgCF_3SO_3$), silver(I) perchlorate hydrate ($AgClO_4 \cdot xH_2O$, $x \sim 1$), or silver(I) hexafluoroantimonate ($AgSbF_6$) produces cyclic dimers of composition $[Ag(\mathbf{1})(X)]_2$ ($X = CF_3SO_3^-$ (**4**) or ClO_4^- (**5**)) and $\{[Ag(\mathbf{1})](SbF_6)\}_2$ (**6**). For these structures, 2,3′-DCPA coordinates to silver(I) ions in a *cisoid* conformation with respect to the orientation of nitrile groups. Significant deformations of the cyclic dimers are observed as a function of the counterion employed. In contrast to the finite structures involving 2,3′-DCPA, crystallization of 2,2′-DCPA (**2**) with $AgCF_3SO_3$ yields the infinite chain structure $[Ag(\mathbf{2})(CF_3SO_3)]$ (**7**). 2,2′-DCPA coordinates to silver(I) in a *transoid* conformation resulting in a "half-bow-tie" motif for the chains. Crystallization of 2,4′-DCPA (**3**) with $AgCF_3SO_3$ produces the infinite, undulating sheet structure $[Ag(\mathbf{3})(CF_3SO_3)]$ (**8**) in which helical chains of 2,4′-DCPA coordinated to silver(I) ions are bridged by triflate counterions. Positive ion ESI-MS of solutions of 2,3′-DCPA (**1**) and $AgCF_3SO_3$, $AgClO_4 \cdot H_2O$, or $AgSbF_6$ in acetone or acetonitrile show a distribution of aggregates including $[Ag_2(\mathbf{1})_2(X)]^+$ ($X = CF_3SO_3^-$, ClO_4^-, or SbF_6^-). The composition of these species corresponds to that of the cyclic dimers of complexes **4**−**6** minus one counterion, X. With 2,2′-DCPA (**2**) and $AgCF_3SO_3$ in acetone or acetonitrile, the aggregates $[Ag(\mathbf{2})]^+$ and $[Ag(\mathbf{2})_2]^+$ are observed and higher adducts are noted to be present in much lower abundance. It is believed that the predominance of adducts involving one silver(I) ion is due to the formation of chelated species in solution in which 2,2′-DCPA coordinates to a silver(I) ion in a *cisoid* conformation. Molecular modeling suggests that such species are viable. ESI-MS of 2,4′-DCPA (**3**) and $AgCF_3SO_3$ in acetone or acetonitrile shows the existence of $[Ag(\mathbf{3})]^+$ as well as higher aggregates which are less prevalent. For a given ligand, aggregation at concentrations of the ligand and silver(I) salt of ca. 10^{-3} M is significant in acetone, however, it is largely disrupted in acetonitrile due to the predominance of acetonitrile·Ag(I) adducts. Analysis of the ESI-MS data for all three ligands with $AgCF_3SO_3$ in acetone or acetonitrile shows that the aggregate $[Ag_2(L)_2(CF_3SO_3)]^+$ is most abundant for L = 2,3′-DCPA (**1**). It is postulated that the relatively high abundance of $[Ag_2(\mathbf{1})_2(CF_3SO_3)]^+$ is indicative of the formation of a cyclic dimer in solution that resembles complex **4**. Similarly, it is believed that cyclic dimers exist in solution with ClO_4^- and SbF_6^- as well.

Introduction

The field of self-assembly, and more specifically crystal engineering, is concerned with controlling the arrangement of molecules via noncovalent interactions to produce aggregates of desired topology, property, and function.[1] Toward this end, metal coordination poses a challenge due to the variable coordination sphere inherent to many ions which is influenced by factors such as counterion, solvent, and ligand geometry (i.e., the relative positioning of coordinating groups). It is therefore of interest to probe the formation of solid-state aggregates as a function of these variables. Another key issue concerning the rational design of coordination networks, and self-assembly in general, is understanding the aggregation process in solution that leads to crystallization. While it is useful to study the packing of structures in the solid state in an attempt to discover trends,[2] little is known about the molecular mechanisms in the crystallization event that lead to observed packing arrangements. It is believed that studies of solution aggregates could provide insight into the crystallization process by drawing a relationship between order in solution and the solid state. Thus, information regarding states of aggregation prior to crystallization would allow for a better understanding of the self-assembly process. For example, can prenucleation species that are structurally related to the eventual solid-state topology be identified in solution? Further, how does the distribution of aggregates depend on concentration and other conditions? Are there

* To whom correspondence should be addressed.
† Department of Chemistry.
‡ Departments of Chemistry and Materials Science and Engineering.
⊗ Abstract published in *Advance ACS Abstracts,* October 1, 1997.

(1) (a) Robson, R.; Abrahams, B. F.; Batten, S. R.; Gable, R. W.; Hoskins, B. F.; Liu, J. In *Supramolecular Architecture*; Bein, T., Ed.; American Chemical Society: Washington, DC, 1992; pp 256−273. (b) Fujita, M.; Kwon, Y. J.; Washizu, S.; Ogura, K. *J. Am. Chem. Soc.* **1994**, *116*, 1151−1152. (c) Gardner, G. B.; Venkataraman, D.; Moore, J. S.; Lee, S. *Nature* **1995**, *374*, 792−795. (d) Venkataraman, D.; Gardner, G. B.; Lee, S.; Moore, J. S. *J. Am. Chem. Soc.* **1995**, *117*, 11600−11601. (e) Yaghi, O. M.; Li, G.; Li, H. *Nature* **1995**, *378*, 703−706.

(2) Hirsch, K. A.; Wilson, S. R.; Moore, J. S. *Chem. Eur. J.* **1997**, *3*, 765−771.

S0002-7863(97)01135-9 CCC: $14.00

significant species present in solution that are unrelated to the observed solid? What causes one or more of these species to be selected and channeled down a pathway to form a crystallization nucleus? In an attempt to begin to address these issues, we report crystal structures of the kinked, ditopic ligands 2,3′-dicyanodiphenylacetylene (2,3′-DCPA, **1**), 2,2′-dicyanodiphenylacetylene (2,2′-DCPA, **2**), and 2,4′-dicyanodiphenylacetylene (2,4′-DCPA, **3**) with silver(I) salts. The topology of these structures is found to depend on the ligand geometry, as finite structures are observed with ligand **1** and infinite structures are formed with ligands **2** and **3**. Solution aggregation of ligands **1**−**3** with silver(I) salts has been probed by electrospray ionization mass spectrometry (ESI-MS)[3] in acetone and acetonitrile. This is the first study to apply ESI-MS to systems that yield infinite coordination networks. Aggregates of the ditopic ligands and silver(I) salts are observed in both solvents; however, aggregation is diminished in acetonitrile due to the predominance of solvent coordination to silver(I). From analysis of the ESI-MS data, structures of key aggregates present in solution are proposed.

Results

Syntheses of 2,3′-Dicyanodiphenylacetylene (2,3′-DCPA, 1), 2,2′-Dicyanodiphenylacetylene (2,2′-DCPA, 2), and 2,4′-Dicyanodiphenylacetylene (2,4′-DCPA, 3). Compounds **1**−**3** were utilized for this study to probe the topology of networks formed through the introduction of "kinks" into the backbone of ditopic ligands. This is in contrast to many studies involving ditopic ligands in which simple, linear rods such as 4,4′-bipyridine are employed.[4] 2,3′- and 2,2′-DCPA were prepared by the three-step sequences outlined in Scheme 1. Palladium-catalyzed cross coupling[5] of (trimethylsilyl)acetylene with 2-bromobenzonitrile afforded trimethylsilyl-protected 2-ethynylbenzonitrile (**9**) in high yield. Deprotection to the terminal acetylene was performed with K_2CO_3 in MeOH and CH_2Cl_2, and the product was not isolated. The formation of 2,3′- and 2,2′-DCPA was achieved in good yield via palladium-catalyzed cross coupling of the terminal acetylene with 3-bromobenzonitrile in the case of the former and 2-bromobenzonitrile in the case of the latter.

2,4′-DCPA was prepared by a similar three-step procedure, shown in Scheme 2. In this case, palladium-catalyzed cross coupling of (trimethylsilyl)acetylene with 4-bromobenzonitrile produced trimethylsilyl-protected 4-ethynylbenzonitrile (**10**) in high yield. Deprotection to 4-ethynylbenzonitrile (**11**) with K_2CO_3 in MeOH and CH_2Cl_2 was nearly quantitative. Palladium-catalyzed cross coupling of acetylene **11** with 2-bromobenzonitrile afforded 2,4′-DCPA in good yield.

Scheme 1. Syntheses of 2,3′- and 2,2′-DCPA (**1** and **2**, Respectively)[a]

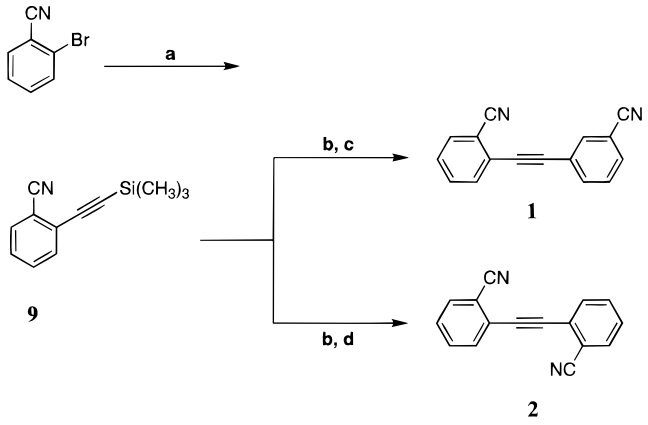

[a] (a) (Trimethylsilyl)acetylene, $Pd(dba)_2$, CuI, Ph_3P, Et_3N, N_2, 75 °C, 21 h, 80%. (b) K_2CO_3, MeOH, CH_2Cl_2, N_2, room temperature, 55 min. (c) 3-Bromobenzonitrile, $Pd(dba)_2$, CuI, Ph_3P, Et_3N, N_2, 77 °C. 21 h 61% (two steps). (d) 2-Bromobenzonitrile, $Pd(dba)_2$, CuI, Ph_3P, Et_3N, N_2, 80 °C, 20 h, 59% (two steps).

Scheme 2. Synthesis of 2,4′-DCPA (**3**)[a]

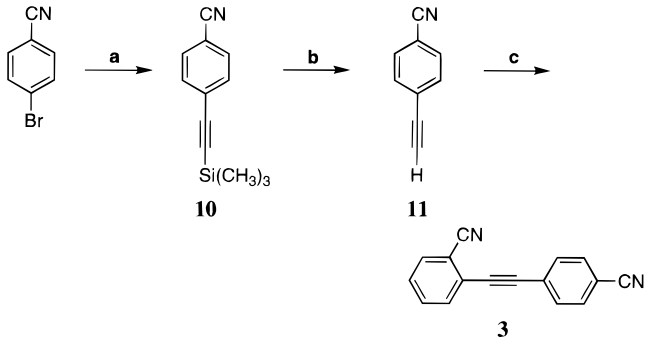

[a] (a) (Trimethylsilyl)acetylene, $Pd(dba)_2$, CuI, Ph_3P, Et_3N, N_2, 75 °C, 16 h, 81%. (b) K_2CO_3, MeOH, CH_2Cl_2, N_2, room temperature, 1.5 h, 97%. (c) 2-Bromobenzonitrile, $Pd(dba)_2$, CuI, Ph_3P, Et_3N, N_2, 75 °C, 24 h, 70%.

Crystallization of Ligands 1−3 with Silver(I) Salts. Compounds **1**−**3** were found to be soluble in common organic solvents at room temperature or with moderate heating which facilitated crystallization with silver(I) salts. For 2,3′-DCPA, crystallization with $AgCF_3SO_3$ and $AgSbF_6$ was achieved in toluene and benzene, respectively, by heating and slow cooling. With $AgClO_4 \cdot H_2O$, crystals suitable for X-ray analysis were obtained by slow evaporation of acetone at room temperature. For 2,2′-DCPA, well-formed crystals with $AgCF_3SO_3$ were obtained in xylenes by heating and slow cooling. Crystallization of 2,4′-DCPA with $AgCF_3SO_3$ was achieved by heating and slow cooling in toluene. Table 1 lists relevant X-ray data for all of the structures characterized.

Crystallization of 2,3′-DCPA (1) with $AgCF_3SO_3$, $AgClO_4 \cdot H_2O$, and $AgSbF_6$: Formation of the Cyclic Dimers $[Ag(1)(CF_3SO_3)]_2$ (4), $[Ag(1)(ClO_4)]_2$ (5), and $\{[Ag(1)](SbF_6)\}_2$ (6). Crystallization of 2,3′-DCPA with $AgCF_3SO_3$, $AgClO_4 \cdot H_2O$, or $AgSbF_6$ produces cyclic dimers of the ditopic ligand and silver(I) salt which are of similar topology. Significant deformations of the dimers are observed as a function of the counterion. With $AgCF_3SO_3$, cyclic dimer **4** is obtained

(3) For studies of noncovalent aggregation by electrospray ionization mass spectrometry, see: (a) Cheng, X.; Gao, Q.; Smith, R. D.; Simanek, E. E.; Mammen, M.; Whitesides, G. M. *J. Org. Chem.* **1996**, *61*, 2204−2206. (b) Fujita, M.; Ibukuro, F.; Hagihara, H.; Ogura, K. *Nature* **1994**, *367*, 720−723. (c) Manna, J.; Whiteford, J. A.; Stang, P. J.; Muddiman, D. C.; Smith, R. D. *J. Am. Chem. Soc.* **1996**, *118*, 8731−8732. (d) Langley, G. J.; Hecquet, E.; Morris, I. P.; Hamilton, D. G. *Rapid Commun. Mass Spectrom.* **1997**, *11*, 165−170. (e) Marquis-Rigault, A.; Dupont-Gervais, A.; Van Dorsselaer, A.; Lehn, J.-M. *Chem. Eur. J.* **1996**, *2*, 1395−1398. (f) Funeriu, D. P.; Lehn, J.-M.; Baum, G.; Fenske, D. *Chem. Eur. J.* **1997**, *3*, 99−104. (g) Moucheron, C.; Kirsch-De Mesmaeker, A.; Dupont-Gervais, A.; Leize, E.; Van Dorsselaer, A. *J. Am. Chem. Soc.* **1996**, *118*, 12834−12835. (h) Przybylski, M.; Glocker, M. O. *Angew. Chem., Int. Ed. Engl.* **1996**, *35*, 806−826.

(4) For examples of coordination networks prepared with 4,4′-bipyridine, see: (a) Carlucci, L.; Ciani, G.; Proserpio, D. M.; Sironi, A. *J. Chem. Soc., Chem. Commun.* **1994**, 2755−2756. (b) MacGillivray, L. R.; Subramanian, S.; Zaworotko, M. J. *J. Chem. Soc., Chem. Commun.* **1994**, 1325−1326. (c) Robinson, F.; Zaworotko, M. J. *J. Chem. Soc., Chem. Commun.* **1995**, 2413−2414. (d) Losier, P.; Zaworotko, M. J. *Angew. Chem., Int. Ed. Engl.* **1996**, *35*, 2779−2782. (e) Yaghi, O. M.; Li, G. *Angew. Chem., Int. Ed. Engl.* **1995**, *34*, 207−209. (f) Yaghi, O. M.; Li, H. *J. Am. Chem. Soc.* **1995**, *117*, 10401−10402. (g) Yaghi, O. M.; Li, H. *J. Am. Chem. Soc.* **1996**, *118*, 295−296.

(5) For examples of the preparation of phenylacetylenes via palladium-catalyzed cross coupling reactions, see: (a) Wu, Z.; Moore, J. S. *Angew. Chem., Int. Ed. Engl.* **1996**, *35*, 297−299. (b) Zhang, J.; Pesak, D. J.; Ludwick, J. L.; Moore, J. S. *J. Am. Chem. Soc.* **1994**, *116*, 4227−4239. (c) Xu, Z.; Moore, J. S. *Angew. Chem., Int. Ed. Engl.* **1993**, *32*, 1354−1357.

Table 1. Crystallographic Data for Complexes **4**−**8**

	[Ag(**1**)(CF_3SO_3)]$_2$ (**4**)	[Ag(**1**)(ClO_4)]$_2$ (**5**)	{[Ag(**1**)](SbF_6)}$_2$ (**6**)	[Ag(**2**)(CF_3SO_3)] (**7**)	[Ag(**3**)(CF_3SO_3)] (**8**)
formula	$C_{17}H_8N_2O_3F_3SAg$	$C_{16}H_8N_2O_4ClAg$	$C_{16}H_8N_2F_6AgSb$	$C_{17}H_8N_2O_3F_3SAg$	$C_{17}H_8N_2O_3F_3SAg$
formula weight	485.18	435.56	571.86	485.18	485.18
crystal system	triclinic	triclinic	triclinic	orthorhombic	monoclinic
space group	$P\bar{1}$ (no. 2)	$P\bar{1}$ (no. 2)	$P\bar{1}$ (no. 2)	*Pnma* (no. 62)	$P2_1/c$ (no. 14)
crystal color	colorless	colorless	colorless	colorless	colorless
unit cell parameters	$a = 9.1222(6)$ Å	$a = 7.509(1)$ Å	$a = 8.620(1)$ Å	$a = 12.913(6)$ Å	$a = 10.5845(9)$ Å
	$b = 10.1711(6)$ Å	$b = 9.815(1)$ Å	$b = 10.547(1)$ Å	$b = 19.849(6)$ Å	$b = 14.5015(3)$ Å
	$c = 10.5369(3)$ Å	$c = 11.220(1)$ Å	$c = 10.815(1)$ Å	$c = 6.892(2)$ Å	$c = 11.9019(9)$ Å
	$\alpha = 63.696(3)°$	$\alpha = 69.995(3)°$	$\alpha = 62.106(6)°$	$\alpha = \beta = \gamma = 90°$	$\alpha = \gamma = 90°$
	$\beta = 84.253(0)°$	$\beta = 80.159(0)°$	$\beta = 88.499(9)°$		$\beta = 100.400(3)°$
	$\gamma = 89.698(3)°$	$\gamma = 83.517(6)°$	$\gamma = 86.486(6)°$		
T (°C)	−75	−75	−75	−75	−75
V (Å^3)	871.17(9)	764.2(2)	867.4(2)	1766(1)	1743.2(2)
Z	2	2	2	4	4
ρ_{calcd} (g cm^{-3})	1.850	1.893	2.190	1.824	1.849
λ (Å) (Mo Kα)	0.71073	0.71073	0.71073	0.71073	0.71073
μ (cm^{-1})	13.28	15.17	27.48	13.10	13.27
unweighted agreement factor ($R1$)[a]	0.0334 ($F_o > 4\sigma$), 0.0424 (all data)	0.0429 ($F_o > 4\sigma$), 0.0576 (all data)	0.0682 ($F_o > 4\sigma$), 0.1116 (all data)	0.0506 ($F_o > 4\sigma$), 0.1140 (all data)	0.0409 ($F_o > 4\sigma$), 0.0644 (all data)
weighted agreement factor ($wR2$)[b]	0.0666 ($F_o > 4\sigma$), 0.0739 (all data)	0.0842 ($F_o > 4\sigma$), 0.0957 (all data)	0.1196 ($F_o > 4\sigma$), 0.1508 (all data)	0.0824 ($F_o > 4\sigma$), 0.1044 (all data)	0.0945 ($F_o > 4\sigma$), 0.1092 (all data)

[a] $R1 = \sum(|F_o| - |F_c|)/\sum|F_o|$. [b] $wR2 = [\sum(w|F_o^2 - F_c^2|)/\sum w|F_o^2|^2]^{1/2}$.

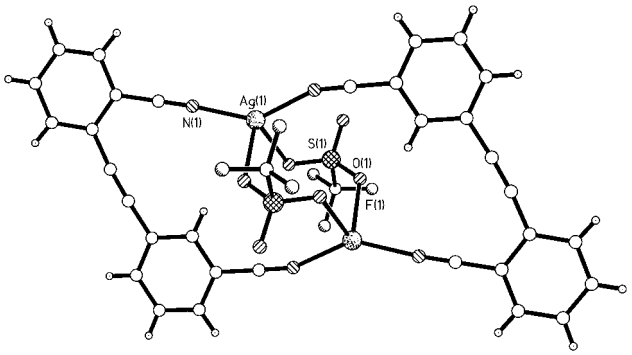

Figure 1. Cyclic dimer [Ag(**1**)(CF_3SO_3)]$_2$ (**4**). 2,3′-DCPA (**1**) coordinates to silver(I) in a *cisoid* conformation. Silver(I) adopts a distorted tetrahedral geometry, coordinating to two oxygen atoms of triflate and two nitrogen atoms of 2,3′-DCPA. Triflate ions bridge across the macrocycle, giving complex **4** a distorted appearance. The N−Ag−N bond angle is 142.8(1)°, and the Ag···Ag distance across the ring is 4.89 Å.

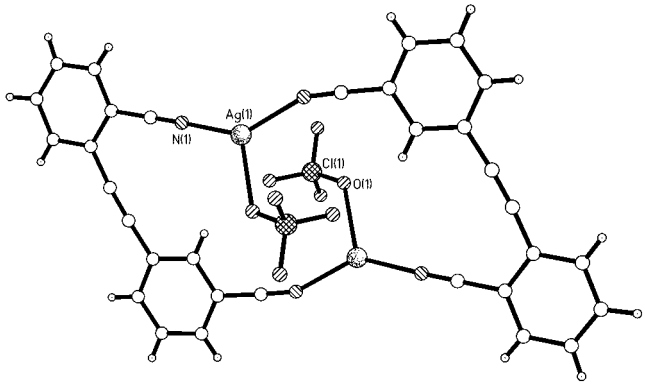

Figure 2. Cyclic dimer [Ag(**1**)(ClO_4)]$_2$ (**5**). Minor site counterion positions have been omitted for clarity. Silver(I) coordinates in a trigonal planar geometry to two nitrogen atoms of 2,3′-DCPA and one oxygen atom of a perchlorate ion. In contrast to complex **4** with triflate, bridging of perchlorate across the macrocycle is not observed. Complex **5** appears distorted as the N−Ag−N bond angle is 138.4(1)°, and the Ag···Ag distance across the ring is 5.08 Å.

from toluene (Figure 1). No solvent is incorporated in the lattice. To form the cyclic motif, 2,3′-DCPA coordinates to silver(I) in a *cisoid* conformation with respect to the orientation of nitrile groups. Each silver(I) ion coordinates to one *meta*-nitrile and one *ortho*-nitrile of the ditopic ligands and overall, silver(I) adopts a distorted tetrahedral geometry through additional bonding to two oxygen atoms of different triflate ions. Thus, each triflate ion bridges two silver(I) ions within a macrocycle through coordination of two oxygen atoms. The Ag−O bond distances are 2.447(2) and 2.464(2) Å. This bridging mode of triflate forms an eight-member ring within a dimer consisting of two triflate ions and two silver(I) ions (Figure 1). As a result of this bridging, the macrocycles appear distorted as the N−Ag−N bond angle is 142.8(1)° and the C−N−Ag bond angles are 158.6(2)° and 172.5(3)°. The N−Ag−N bond angles are contracted toward one another across the macrocycle, and the Ag···Ag distance across the ring is 4.89 Å. The dimers pack in layers allowing $\pi-\pi$ stacking of 2,3′-DCPA molecules of adjacent rings. In this arrangement, $\pi-\pi$ stacking of 2,3′-DCPA is observed along the *a*-axis at a plane-to-plane distance of 3.37 Å.

The packing of cyclic dimer **5** obtained with $AgClO_4 \cdot H_2O$ from acetone is similar to that with $AgCF_3SO_3$. Once again, no solvent is included in the lattice. Interestingly, perchlorate ions coordinate to silver(I) in this structure. Recent examples of coordination networks involving perchlorate have shown this ion to be noncoordinating.[6] Silver(I) adopts a trigonal planar geometry in complex **5**, bonding to two ligand nitrogen atoms and an oxygen atom of a disordered perchlorate ion (Figure 2). The perchlorate ions are disordered over two sites with a major site occupancy of 0.60. The Ag−O bond distance is 2.45(2) Å (counterion oxygen atoms in both the major and minor site bond at this distance). The next closest Ag···O distance across the dimer is 2.75 Å such that bridging of perchlorate is not observed (Figure 2). The macrocycle in complex **5** "relaxes" somewhat in the plane relative to structure **4** since the perchlorate ions do not bridge. As a result, the Ag···Ag distance across a dimer is 5.08 Å in structure **5** as compared to 4.89 Å for complex **4**. However, the N−Ag−N bond angles are 138.4(1)° and are bent

(6) (a) Hirsch, K. A.; Wilson, S. R.; Moore, J. S. *Inorg. Chem.* **1997**, *36*, 2960−2968. (b) Munakata, M; Wu, L. P.; Yamamoto, M.; Kuroda-Sowa, T.; Maekawa, M. *J. Am. Chem. Soc.* **1996**, *118*, 3117−3124. (c) Kuroda-Sowa, T.; Yamamoto, M.; Munakata, M.; Seto, M.; Maekawa, M. *Chem. Lett.* **1996**, 349−350. (d) Munakata, M.; Kitagawa, S.; Ujimura, N.; Nakamura, M.; Maekawa, M; Matsuda, H. *Inorg. Chem.* **1993**, *32*, 826−832. For an example of a network containing a coordinating perchlorate ion, see: Darriet, J.; Haddad, M. S.; Duesler, E. N.; Hendrickson, D. N. *Inorg. Chem.* **1979**, *18*, 2679−2682.

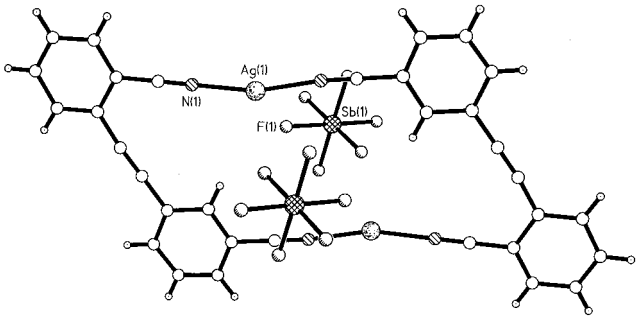

Figure 3. Cyclic dimer $\{[Ag(\mathbf{1})](SbF_6)\}_2$ (**6**). In contrast to complexes **4** and **5** with triflate and perchlorate, respectively, the hexafluoroantimonate ion does not coordinate to silver(I) in complex **6**. As a result, silver(I) coordinates approximately in a linear fashion to two nitrogen atoms of 2,3′-DCPA. The N−Ag−N bond angle is 165.4(5)°, and the macrocycle appears less distorted relative to complexes **4** and **5** (compare to Figures 1 and 2). For complex **6**, the Ag···Ag distance across the ring is 6.05 Å.

out of the plane (one above and one below). The C−N−Ag bond angles are 156.4(3)° and 176.1(3)°, which are similar to those observed in complex **4**. $\pi-\pi$ Stacking of 2,3′-DCPA between an *ortho*-substituted ring and a *meta*-substituted ring is observed at a plane-to-plane distance of 3.41 Å.

Cyclic dimer **6** was obtained with $AgSbF_6$ from benzene, and as with complexes **4** and **5**, contains no solvent. The hexafluoroantimonate ions do not coordinate to silver(I) (Figure 3) as the closest Ag···F contact is 2.67 Å. Thus, silver(I) is simply two-coordinate, bonding to two nitrogen atoms of 2,3′-DCPA. The silver(I) coordination geometry is approximately linear as the N−Ag−N bond angle is 165.4(5)°. As a result of the expansion of the N−Ag−N bond angles in complex **6** relative to complexes **4** and **5**, the Ag···Ag separation across a macrocycle is elongated to 6.05 Å. Also, the C−N−Ag bond angles are both nearly linear (174(1)° and 176(1)°) in contrast to complexes **4** and **5** where one such angle in each structure is bent significantly (158.6(2)° and 156.4(3)° for complexes **4** and **5**, respectively). Overall, the macrocycle in the $AgSbF_6$ structure appears much less distorted (compare Figures 1−3). $\pi-\pi$ Stacking of 2,3′-DCPA is observed at a plane-to-plane distance of 3.40 Å.

In comparing complexes **4**−**6**, it is interesting to note that the cyclic dimer topology is maintained in the presence of three counterions of different size and affinity for silver(I). The coordination number of silver(I) is 2 in the presence of hexafluoroantimonate, 3 with perchlorate, and 4 with triflate. Thus, flexibility of the silver(I) coordination sphere, which is a manifestation of differences in counterion affinity, allows distortions in the macrocyclic framework so as to achieve closest-packing. This is evidenced by consideration that the Ag···Ag distance across a macrocycle in the three structures varies from ca. 4.9 to 6.0 Å.

Crystallization of 2,2′-DCPA (2) with $AgCF_3SO_3$: Formation of the Infinite, "Half-Bow-Tie" Structure [Ag(2)-(CF_3SO_3)] (7). In contrast to the finite structures obtained with 2,3′-DCPA, crystallization of 2,2′-DCPA with $AgCF_3SO_3$ from xylenes produces the infinite chain structure [Ag(**2**)CF_3SO_3] (**7**). This structure crystallizes in the orthorhombic space group *Pnma* (see Table 1), and no solvent is included in the lattice. 2,2′-DCPA coordinates in a *transoid* conformation to silver(I) ions. The kinked nature of the ditopic ligand in this conformation produces chains with a "half-bow-tie" motif as shown in Figure 4.

Silver(I) displays a distorted trigonal planar geometry in complex **7**, bonding to two ligand nitrogen atoms and an oxygen atom of triflate. The N−Ag−N bond angle is 149.0(3)°, and the O−Ag−N bond angles are 94.3(3)° and 114.5(3)°. The triflate counterions are disordered about the mirror plane perpendicular to the *b* axis. The chains are flat, although alternating triflate ions lie above and below the plane consisting of 2,2′-DCPA and silver(I) ions. Neighboring chains layer with "crests" aligned as shown in Figure 5. In this arrangement, $\pi-\pi$ stacking of 2,2′-DCPA is observed with a lateral offset at a plane-to-plane distance of 3.49 Å. The layers pack in an

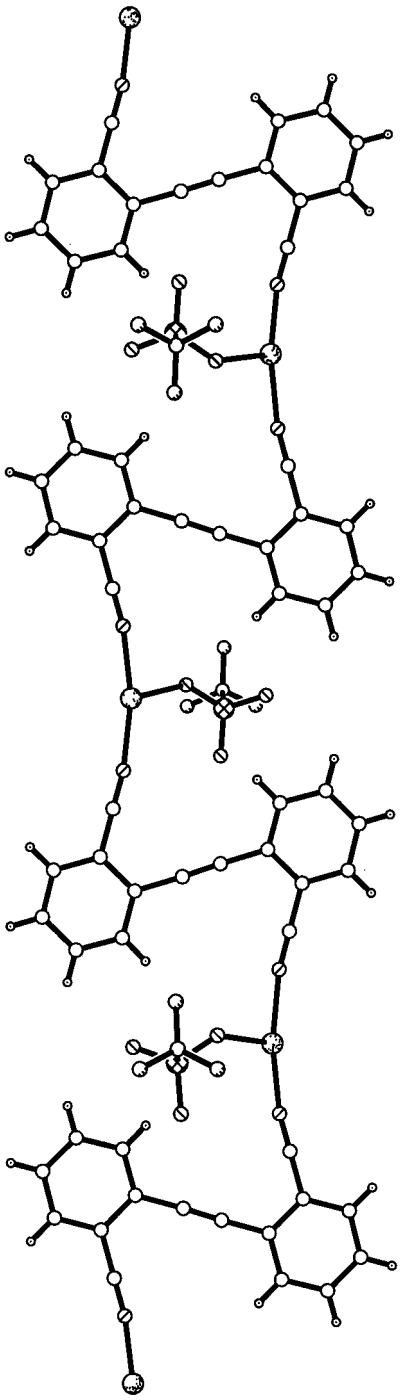

Figure 4. Portion of the infinite chain structure [Ag(**2**)(CF_3SO_3)] (**7**). The triflate ions are disordered about mirror planes running horizontally, and only one triflate site is shown for clarity. 2,2′-DCPA (**2**) coordinates in a *transoid* conformation to silver(I). The chains display a "half-bow-tie" motif as a result of the kinks inherent to 2,2′-DCPA. Silver(I) coordinates in a distorted trigonal planar geometry to two nitrogen atoms of 2,2′-DCPA and one oxygen atom of triflate.

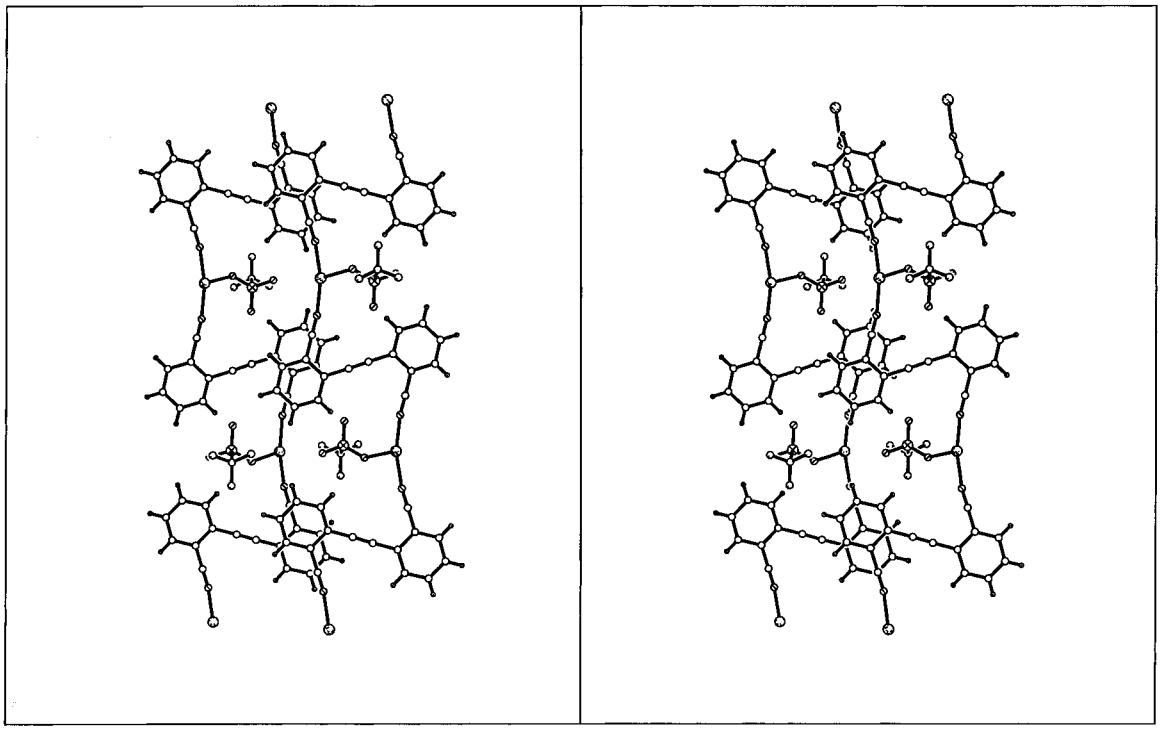

Figure 5. Stereoview highlighting $\pi-\pi$ stacking of 2,2′-DCPA (**2**) in [Ag(**2**)(CF_3SO_3)] (**7**). For each triflate ion, only one site is shown for clarity. Chains pack in layers such that "crests" are aligned. In this arrangement, $\pi-\pi$ stacking of 2,2′-DCPA is observed with a lateral offset at a plane-to-plane distance of 3.49 Å.

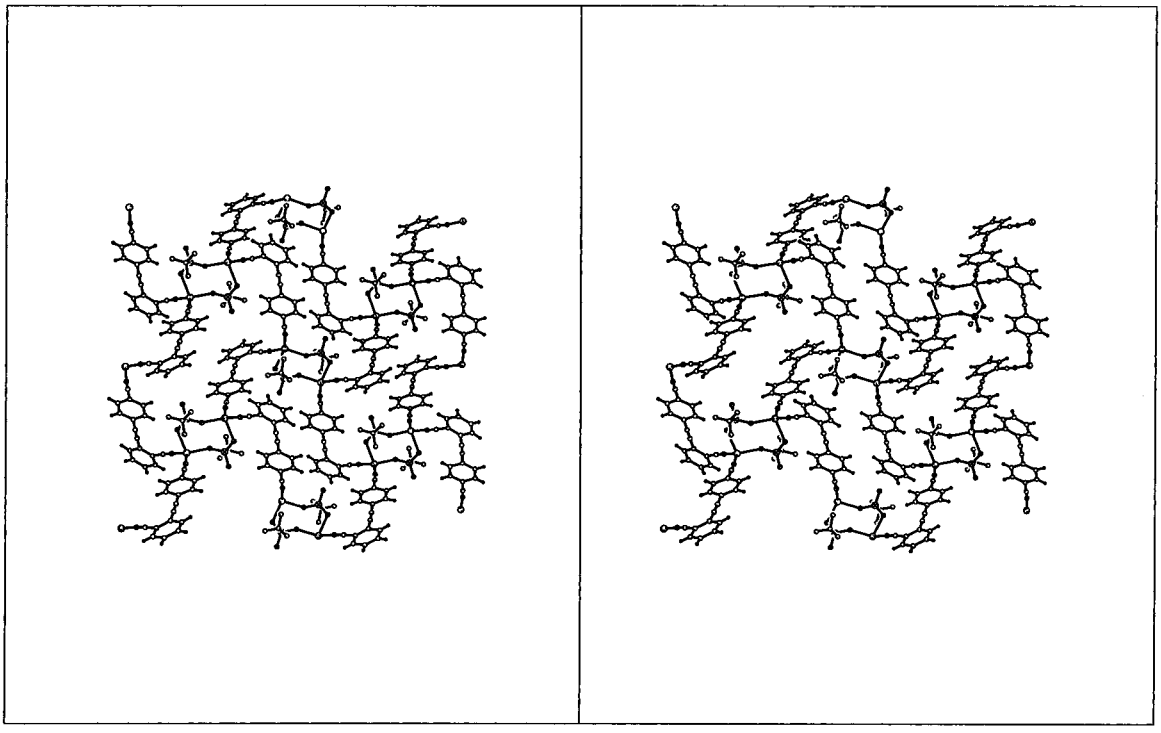

Figure 6. Stereoview of an undulating sheet of [Ag(**3**)(CF_3SO_3)] (**8**). Formation of the sheet may be envisioned by bridging 2/1 helices consisting of the ditopic ligand and silver(I) with triflate ions. Bridged helices are of opposite handedness. Silver(I) adopts a distorted tetrahedral geometry, bonding to two ligand nitrogen atoms and two triflate oxygen atoms.

A·B·A·B fashion to accommodate the triflate ions and to allow offset stacking of 2,2′-DCPA.

Crystallization of 2,4′-DCPA (3) with $AgCF_3SO_3$: Formation of the Infinite, Undulating Sheet Structure [Ag(3)(CF_3SO_3)] (8). Crystallization of 2,4′-DCPA with $AgCF_3SO_3$ from toluene produces the 1:1 adduct [Ag(**3**)(CF_3SO_3)] (**8**) which is an infinite sheet structure. The undulating sheet topology of complex **8** is realized by the bridging of helical chains of 2,4′-DCPA and silver(I) by triflate counterions as illustrated in Figure 6. For this sheet structure, it is noted that bridged helices are of opposite handedness. Two oxygen atoms of triflate bridge adjacent helices via silver(I) coordination. Silver(I), therefore, is four-coordinate and adopts a distorted tetrahedral geometry, bonding to two nitrogen atoms of 2,4′-DCPA and two oxygen atoms of triflate ions. Bond angles about silver(I) range from 92.7(1)° (an O−Ag−N angle) to

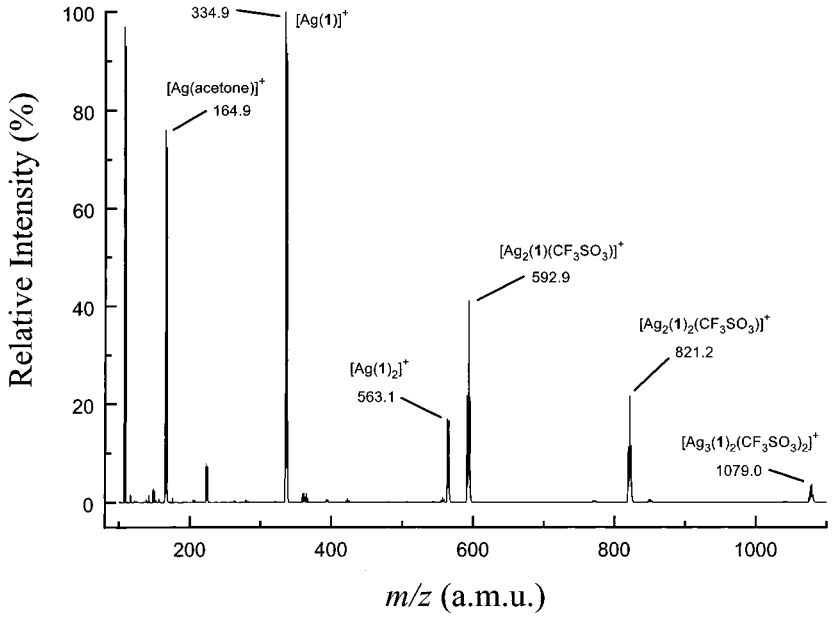

Figure 7. ESI mass spectrum of 2,3′-DCPA (**1**) and $AgCF_3SO_3$ in acetone at concentrations of 1.5 and 1.6 × 10^{-3} M for the ligand and silver(I) salt, respectively. Compositions of the aggregates are labeled. Note that the species at *m*/*z* 821.2 corresponds to removal of a triflate ion from the cyclic dimer observed in complex **4**.

132.4(1)° (the N−Ag−N angle). The bridging mode of triflate observed in complex **8** produces eight-member rings between helices (Figure 6) that are similar to those seen in complex **4** (Figure 1). The Ag···Ag distance across a ring is 4.77 Å. Careful consideration of Figure 6 reveals larger rings within the sheet framework. The circuit of such a ring may be traversed in a Ag^+−**3**−Ag^+−$CF_3SO_3^-$−Ag^+−**3**−Ag^+−**3**−Ag^+−$CF_3SO_3^-$−Ag^+−**3** sequence. Void space within these large rings is filled by the interdigitation of a second sheet. In this arrangement, $\pi-\pi$ stacking of 2,4′-DCPA is observed with a lateral offset at a plane-to-plane distance of 3.41 Å.

Electrospray Ionization Mass Spectrometry (ESI-MS) of Solutions of Ligands 1−3 with Silver(I) Salts. ESI-MS has emerged as a powerful technique for investigating solution aggregation of noncovalent species.[3] For example, Whitesides et al. have used ESI-MS to determine, definitively, the stoichiometry of cyanuric acid−melamine aggregates which had been characterized previously by less direct means such as NMR spectroscopy and vapor pressure osmometry.[3a] For our purposes, ESI-MS was used to probe the existence of aggregates of ligands **1**−**3** with silver(I) salts in solution. Moreover, it was of interest to compare the solution aggregation behavior for systems known to form finite solid-state structures (e.g., those with ligand **1**) and systems that form infinite frameworks (e.g., those with ligands **2** and **3**). For all three ligands, spectra were collected at concentrations of the ligand and silver(I) salt of (1.5−1.6) × 10^{-3} M in acetone or acetonitrile to probe aggregate formation as a function of solvent. Although it was not possible to obtain ESI mass spectra in the nonpolar solvents from which crystals of **4** and **6**−**8** were grown, it is important to note that none of the crystal structures presented here show solvent incorporation which would influence the packing. ESI-MS experiments were performed for these systems in the solvents used for crystallization (i.e., benzene, toluene, or xylenes) and no ions were observed. However, the crystal of complex **5** was grown from acetone and the ESI-MS spectra for complexes **4**−**6** in acetone were compared and the distribution of aggregates is similar for the three spectra (vide infra). For the 2,3′- and 2,2′-DCPA ligands and silver(I) salts, spectra were collected in acetonitrile at higher concentrations (approximately 1.5 × 10^{-2} M in each component) to investigate the effect of concentration on aggregate formation in a competitive solvent. For 2,4′-DCPA, ESI-MS in acetonitrile was not performed at higher concentration due to insolubility of the ligand. For the discussion below, concentrations of the ligand and silver(I) salt are (1.5−1.6) × 10^{-3} M, except where noted otherwise. Comparison of the ESI-MS data among the three ligands provides information about the relative distribution of aggregates.

ESI-MS of 2,3′-DCPA (1) with $AgCF_3SO_3$, $AgClO_4\cdot H_2O$, and $AgSbF_6$: Evidence for the Formation of Dimers in Solution. Positive ion ESI-MS of 2,3′-DCPA and silver(I) salts in both acetone and acetonitrile provides evidence for solution aggregation of 2,3′-DCPA with silver(I) even at fairly dilute concentrations. Moreover, positively charged aggregates with compositions corresponding to $[Ag_2(\mathbf{1})_2(X)]^+$ (X = $CF_3SO_3^-$, ClO_4^-, or SbF_6^-) are observed which are consistent with the dimer motif of crystal structures **4**−**6** (less one counterion).

ESI-MS of 2,3′-DCPA and $AgCF_3SO_3$ in acetone shows the presence of several singly charged species (Figure 7). Complexation of acetone with silver(I) is observed at *m*/*z* 222.9 ($[Ag(acetone)_2]^+$) and *m*/*z* 164.9 ($[Ag(acetone)]^+$). Importantly, an abundant adduct corresponding to $[Ag_2(\mathbf{1})_2(CF_3SO_3)]^+$ is observed at *m*/*z* 821.2. This ion has the composition of the cyclic dimer of complex **4** minus one triflate ion, although we cannot rule out the possibility that some fraction of this peak corresponds to the open chain form. The isotopic distribution observed for this species is in good agreement with the calculated composition (Figures 1 and 2 in the Supporting Information).

The ESI mass spectrum of 2,3′-DCPA and $AgCF_3SO_3$ in acetone also shows other aggregates of these two components. As noted in Figure 7 above, the following species can be identified: *m*/*z* 592.9, $[Ag_2(\mathbf{1})(CF_3SO_3)]^+$; *m*/*z* 563.1, $[Ag(\mathbf{1})_2]^+$; *m*/*z* 334.9, $[Ag(\mathbf{1})]^+$. The higher aggregate $[Ag_3(\mathbf{1})_2(CF_3SO_3)_2]^+$ at *m*/*z* 1079.0 can also be detected. The isotopic distribution of these species is in accord with the calculated composition. Thus, although acetone coordinates to silver(I), aggregation of 2,3′-DCPA and $AgCF_3SO_3$ in this solvent is significant even at millimolar concentrations.

The structural integrity of aggregates of 2,3′-DCPA and $AgCF_3SO_3$ was further probed in acetonitrile, which was

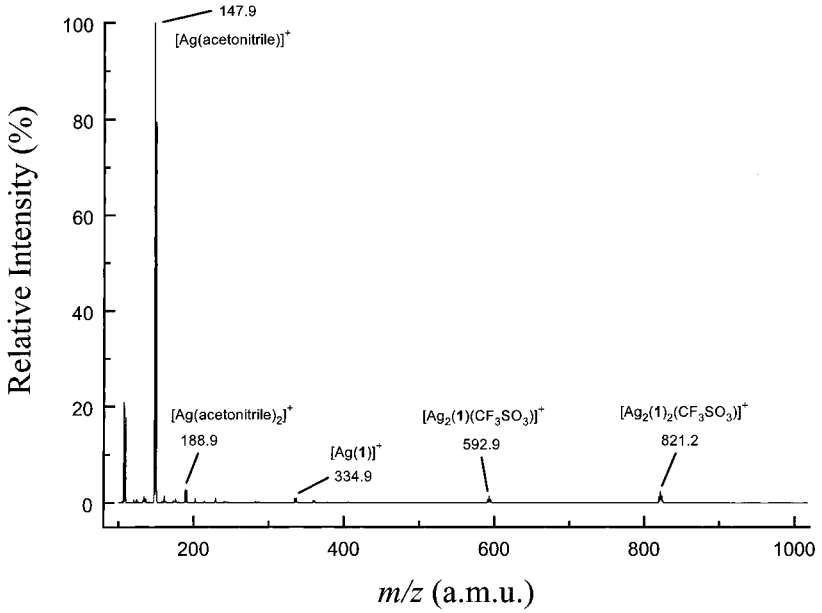

Figure 8. ESI mass spectrum of 2,3′-DCPA (**1**) and $AgCF_3SO_3$ in acetonitrile at concentrations of 1.5 and 1.6×10^{-3} M for the ligand and silver(I) salt, respectively. Compositions of observed aggregates are labeled. The aggregation of 2,3′-DCPA with $AgCF_3SO_3$ is limited due to competition from acetonitrile. Despite the large excess of acetonitrile present, aggregates of 2,3′-DCPA and $AgCF_3SO_3$ are detected, including the dimer at *m/z* 821.2. This spectrum should be compared to the one taken in acetone shown in Figure 7.

expected to behave as a competitive ligand for silver(I). Perhaps not surprisingly, the ESI mass spectrum in acetonitrile shown in Figure 8 is dramatically different than that observed in acetone (Figure 7). The primary species in acetonitrile is noted at *m/z* 147.9 and corresponds to a 1:1 adduct of the solvent and silver(I) ($[Ag(acetonitrile)]^+$; Figure 8). Although far less abundant, the higher adduct $[Ag(acetonitrile)_2]^+$ is also observed at *m/z* 188.9. What is surprising is that, despite the large excess of acetonitrile present, aggregation of 2,3′-DCPA with silver(I) is still observed. It is further noteworthy that the dimer $[Ag_2(\mathbf{1})_2(CF_3SO_3)]^+$ at *m/z* 821.2 is the most abundant adduct involving 2,3′-DCPA in acetonitrile. Thus, ESI-MS shows the formation of a species corresponding to a positively charged cyclic dimer of complex **4** even in the presence of a highly competitive solvent. Other aggregates of 2,3′-DCPA that are observed are $[Ag_2(\mathbf{1})(CF_3SO_3)]^+$ at *m/z* 592.9 and $[Ag(\mathbf{1})]^+$ at *m/z* 334.9. The higher aggregate $[Ag_3(\mathbf{1})_2(CF_3SO_3)_2]^+$ is not observed in acetonitrile. The diminished aggregation of 2,3′-DCPA in acetonitrile may be likened to the decrease in association constant observed in complementary hydrogen bonded systems in the presence of competitive, hydrogen bonding solvents such as DMSO.[7]

ESI-MS of 2,3′-DCPA and $AgClO_4 \cdot H_2O$ shows aggregation behavior similar to that observed with $AgCF_3SO_3$. In acetone, for example, the dimer $[Ag_2(\mathbf{1})_2(ClO_4)]^+$ is noted at *m/z* 771.1 (Figure 3 in the Supporting Information). The isotopic distribution of this species is in good agreement with the calculated distribution (Figures 4 and 5 in the Supporting Information). This aggregate, which has the composition of cyclic dimer **5** minus a perchlorate ion, is observed in acetone, the same solvent used to grow crystals of complex **5**. Other species of interest are those at *m/z* 979.0 ($[Ag_3(\mathbf{1})_2(ClO_4)_2]^+$), 563.1 ($[Ag(\mathbf{1})_2]^+$), 542.9 ($[Ag_2(\mathbf{1})(ClO_4)]^+$), and 334.9 ($[Ag(\mathbf{1})]^+$). In acetonitrile, as with the $AgCF_3SO_3$ example, aggregation of the solvent with silver(I) dominates. However, the dimer at *m/z* 771.1 is observed in acetonitrile (Figure 6 in the Supporting Information).

For 2,3′-DCPA with $AgSbF_6$, ESI-MS in acetone shows the presence of a dimer of composition $[Ag_2(\mathbf{1})_2(SbF_6)]^+$ at *m/z* 907.1 (Figure 7 in the Supporting Information). The isotopic distribution for this species is similar to that calculated (Figures 8 and 9 in the Supporting Information). Other relevant aggregates that can be identified are at *m/z* 678.9 ($[Ag_2(\mathbf{1})(SbF_6)]^+$), 563.1 ($[Ag(\mathbf{1})_2]^+$), and 334.9 ($[Ag(\mathbf{1})]^+$). In acetonitrile, the dimer $[Ag_2(\mathbf{1})_2(SbF_6)]^+$ at *m/z* 907.1 is present in very small amounts due to solvent coordination (Figure 10 in the Supporting Information).

ESI-MS data was also collected for 2,3′-DCPA with $AgCF_3SO_3$, $AgClO_4 \cdot H_2O$, or $AgSbF_6$ in acetonitrile at higher concentrations of the ditopic ligand and silver(I) salt (ca. 1.5×10^{-2} M). For all three salts, the relative abundance of the dimer $[Ag_2(\mathbf{1})_2X]^+$ (X = $CF_3SO_3^-$, ClO_4^-, or SbF_6^-) increases at higher concentration. At the higher concentration, the relative abundance of the dimers is greater than the lower aggregates containing one silver(I) ion (Figures 11−13 in the Supporting Information for $CF_3SO_3^-$, ClO_4^-, and SbF_6^-, respectively). This observation is consistent the formation of stable cyclic dimers involving 2,3′-DCPA in solution.[8]

ESI-MS of 2,2′-DCPA (2) with $AgCF_3SO_3$. ESI-MS was used to probe the existence of solution aggregates for ligands known to form infinite structures in the solid state. With 2,2′-DCPA and $AgCF_3SO_3$, the aggregation behavior is different than was observed with 2,3′-DCPA. In acetone, the 1:1 adduct of 2,2′-DCPA and silver(I), $[Ag(\mathbf{2})]^+$, predominates at *m/z* 334.9 (Figure 9). Also, a species corresponding to $[Ag(\mathbf{2})_2]^+$ is noted at *m/z* 563.1 which is comparable in intensity to the $[Ag(acetone)]^+$ ion. Interestingly, the higher aggregates $[Ag_2(\mathbf{2})(CF_3SO_3)]^+$ (*m/z* 592.9) and $[Ag_2(\mathbf{2})_2(CF_3SO_3)]^+$ (*m/z* 821.2) are present in very low abundance (the spectrum in Figure 9 should be compared to the spectrum of 2,3′-DCPA and $AgCF_3SO_3$ in acetone shown in Figure 7). It is believed that the predominance of the $[Ag(\mathbf{2})]^+$ aggregate is a result of chelation of 2,2′-DCPA to silver(I) (i.e., coordination of 2,2′-DCPA in a *cisoid* conformation similar to the coordination mode often observed for 2,2′-bipyridine). Molecular modeling suggests that chelation

(7) Bell, T. W.; Hou, Z.; Zimmerman, S. C.; Thiessen, P. A. *Angew. Chem., Int. Ed. Engl.* **1995**, *34*, 2163-2165.

(8) For examples of cyclic aggregates characterized by ESI-MS, see refs 3b and 3c.

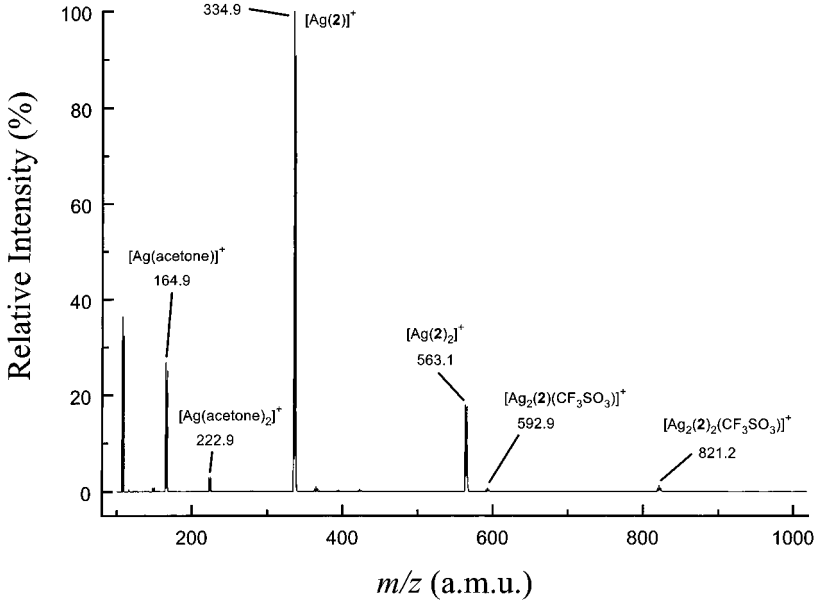

Figure 9. ESI mass spectrum of 2,2′-DCPA (**2**) and $AgCF_3SO_3$ in acetone. Compositions of observed aggregates are labeled. Note that the abundance of higher aggregates involving two silver(I) ions (i.e., those at *m*/*z* 592.9 and 821.2) is lower than was observed for 2,3′-DCPA and $AgCF_3SO_3$ in acetone (see Figure 7). This is likely a result of chelation of 2,2′-DCPA to silver(I).

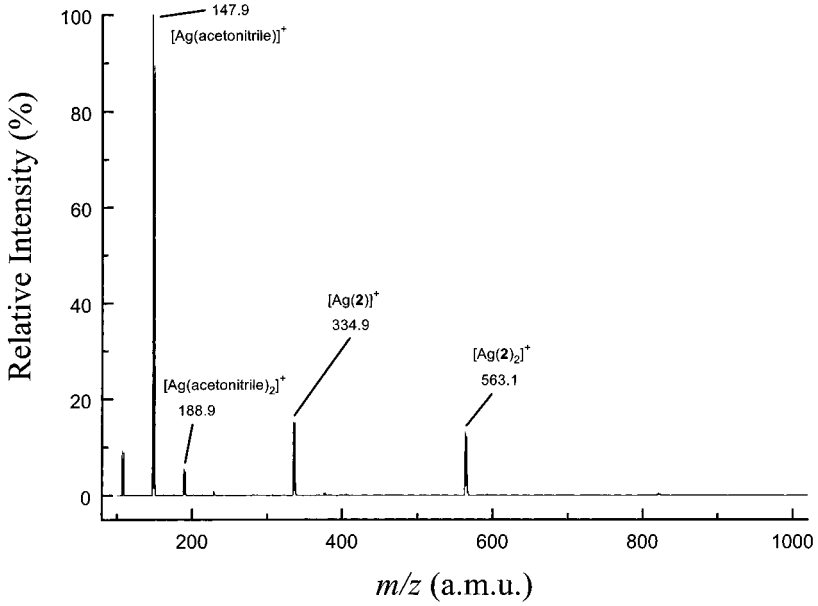

Figure 10. ESI mass spectrum of 2,2′-DCPA (**2**) and $AgCF_3SO_3$ in acetonitrile at concentrations of 1.5 and 1.6 × 10^{-3} M for the ligand and silver(I) salt, respectively. Compositions of the aggregates are denoted. Aggregation involving 2,2′-DCPA is reduced due to competition of acetonitrile for silver(I). However, in acetonitrile, the abundance of the species $[Ag(\mathbf{2})]^+$ at *m*/*z* 334.9 is much greater than the abundance of adducts involving 2,3′-DCPA (compare to Figure 8). This likely reflects chelation of 2,2′-DCPA to silver(I).

is reasonable for 2,2′-DCPA.[9] It is likely that chelation stabilizes the $[Ag(\mathbf{2})]^+$ species by allowing silver(I) to be two-coordinate rather than one-coordinate which would result from coordination of 2,2′-DCPA in a *transoid* conformation. It should also be noted that, for the $[Ag(\mathbf{2})_2]^+$ adduct, molecular modeling suggests that two 2,2′-DCPA molecules are capable of coordinating in a *cisoid* conformation to a distorted tetrahedral silver(I) ion.[9]

For ESI-MS of 2,2′-DCPA and $AgCF_3SO_3$ in acetonitrile, the 1:1 adduct of the solvent and silver(I) ($[Ag(acetonitrile)]^+$, *m*/*z* 147.9) is the predominant species observed (Figure 10). The adduct $[Ag(acetonitrile)_2]^+$ at *m*/*z* 188.9 is also noted. The aggregate $[Ag(\mathbf{2})]^+$ at *m*/*z* 334.9 is observed in acetonitrile, although this species is less abundant than in acetone (Figure 9). In fact, in acetonitrile, the 2:1 2,2′-DCPA·Ag(I) adduct $[Ag(\mathbf{2})_2]^+$ at *m*/*z* 563.1 is nearly as abundant as the 1:1 adduct at *m*/*z* 334.9. The higher aggregate at *m*/*z* 821.2 ($[Ag_2(\mathbf{2})_2(CF_3SO_3)]^+$) is only present in trace amounts. In acetonitrile, aggregates involving 2,2′-DCPA and one silver(I) ion are more abundant than those of 2,3′-DCPA (compare Figures 8 and 10), which again points toward chelation of the 2,2′-DCPA ligand.

ESI-MS of 2,2′-DCPA and $AgCF_3SO_3$ was also performed in acetonitrile at concentrations of ca. 1.5 × 10^{-2} M for the two components (as compared to millimolar concentrations for the spectrum shown in Figure 10). At the higher concentration, the $[Ag(\mathbf{2})]^+$ adduct predominates over $[Ag(acetonitrile)]^+$ (Figure 11) in contrast to the behavior seen at the lower

(9) Molecular modeling was performed with Cerius^2, version 2.0: Molecular Simulations, Inc., San Diego, CA, 1995. Universal Force Field 1.01 was employed: Rappe, A. K.; Casewit, C. J.; Colwell, K. S.; Goddard, W. A., III; Skiff, W. M. *J. Am. Chem. Soc.* **1992**, *114*, 10024−10035.

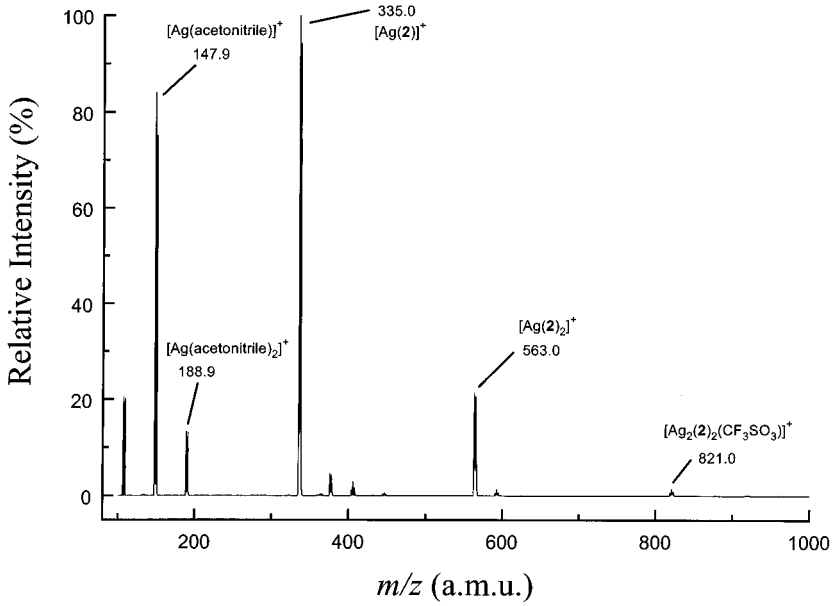

Figure 11. ESI mass spectrum of 2,2′-DCPA (**2**) and $AgCF_3SO_3$ in acetonitrile at concentrations of 1.5×10^{-2} M for the ligand and silver(I) salt. Compositions of the aggregates are denoted. In this case, the adduct $[Ag(\mathbf{2})]^+$ at *m*/*z* 335.0 predominates over the [Ag(acetonitrile)]$^+$ species at *m*/*z* 147.9. This result further suggests chelation of the ditopic ligand to silver(I). This spectrum should be compared to the one of 2,2′-DCPA and $AgCF_3SO_3$ obtained in acetonitrile at millimolar concentrations (Figure 10).

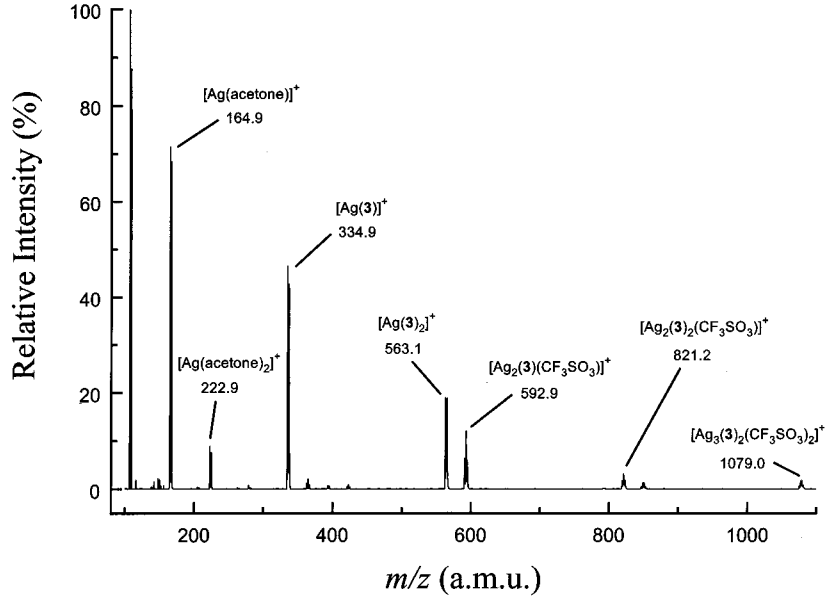

Figure 12. ESI mass spectrum of 2,4′-DCPA (**3**) and $AgCF_3SO_3$ in acetone at concentrations of 1.5×10^{-3} and 1.6×10^{-3} M for the ligand and silver(I) salt, respectively. Compositions of the observed aggregates are denoted. The aggregation behavior of 2,4′-DCPA is similar to that shown for 2,3′-DCPA and $AgCF_3SO_3$ in acetone (see Figure 7).

concentration (compare Figures 10 and 11). The abundance of the $[Ag(\mathbf{2})]^+$ species in a competitive solvent further suggests chelation of 2,2′-DCPA to silver(I) in solution.

ESI-MS of 2,4′-DCPA (3) with $AgCF_3SO_3$. The aggregation behavior of 2,4′-DCPA and $AgCF_3SO_3$ is similar to that described for 2,3′-DCPA and $AgCF_3SO_3$. In acetone, the predominant species present involving 2,4′-DCPA is a 1:1 adduct $[Ag(\mathbf{3})]^+$ at *m*/*z* 334.9 (Figure 12). Also observed are adducts at *m*/*z* 563.1 ($[Ag(\mathbf{3})_2]^+$), 592.9 ($[Ag_2(\mathbf{3})(CF_3SO_3)]^+$), 821.2 ($[Ag_2(\mathbf{3})_2(CF_3SO_3)]^+$), and 1079.0 ($[Ag_3(\mathbf{3})_2(CF_3SO_3)_2]^+$).

In acetonitrile, aggregation of 2,4′-DCPA is nearly completely disrupted (Figure 14 in the Supporting Information). The primary species observed are [Ag(acetonitrile)]$^+$ at *m*/*z* 147.9 and $[Ag(acetonitrile)_2]^+$ at *m*/*z* 188.9. Only trace amounts of aggregates involving 2,4′-DCPA are detected at *m*/*z* 334.9, 563.1, 592.9, and 821.2.

Discussion

It is not yet clear how quantitative ESI-MS is at representing the relative distribution of species in a solution equilibrium.[3d,h] Of course, ESI-MS only samples charged species transferred from solution to the gas phase. Even so, our findings suggest that, at least qualitatively, the expected trends were observed (i.e., ligand aggregation is stronger in acetone than acetonitrile at the same concentration and the aggregates are more abundant at higher concentration). Noteworthy trends regarding the relative solution aggregation of 2,2′-, 2,3′-, and 2,4′-DCPA with silver(I) were discussed in the previous section. From the ESI-MS results, it was suggested that, for 2,2′-DCPA (**2**), the predominance of the $[Ag(\mathbf{2})]^+$ adduct reflects chelation of the ligand to silver(I) in solution. Further, the high relative abundance of the aggregate $[Ag_2(\mathbf{1})_2(CF_3SO_3)]^+$ was attributed

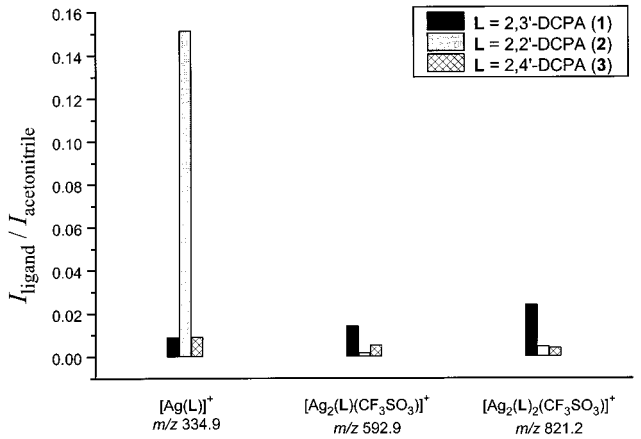

Figure 13. Plot showing abundances of key aggregates of ditopic ligands **1**−**3** and $AgCF_3SO_3$ in acetonitrile relative to the abundance of the $[Ag(acetonitrile)]^+$ adduct (*m*/*z* 147.9) observed in each spectrum. The plot was constructed for data collected at concentrations of 1.5×10^{-3} and 1.6×10^{-3} M for the ligand and silver(I) salt, respectively. As shown, for 2,2′-DCPA (**2**), the adduct $[Ag(\mathbf{2})]^+$ (*m*/*z* 334.9) predominates over higher adducts and over $[Ag(\mathbf{1})]^+$ and $[Ag(\mathbf{3})]^+$. This comparison further suggests that 2,2′-DCPA chelates to silver(I) in solution. Also noteworthy is the observation that the dimer $[Ag_2(L)_2(CF_3SO_3)]^+$ (*m*/*z* 821.2) is most abundant for L = 2,3′-DCPA (**1**). This further points to the formation of cyclic dimers in solution with 2,3′-DCPA that resemble the cyclic motif in crystal structures **4**−**6**. For 2,4′-DCPA (**3**), it is noted that the abundance of the $[Ag(\mathbf{3})]^+$ species is much lower than that of $[Ag(\mathbf{2})]^+$. This is likely a result of the inability of 2,4′-DCPA to chelate to silver(I). Further, the abundance of higher aggregates involving 2,4′-DCPA is lower than those with 2,3′-DCPA. It is believed that this is due to the inability of 2,4′-DCPA to form cyclic adducts.

to formation of a cyclic dimer involving 2,3′-DCPA (**1**) in solution. To fortify these points, a plot of the abundance of key aggregates of the three ligands with $AgCF_3SO_3$ in acetonitrile relative to the abundance of the $[Ag(acetonitrile)]^+$ adduct (*m*/*z* 147.9) is shown in Figure 13. This plot represents data collected at millimolar concentrations. The plot reveals noteworthy aggregation behavior as a function of the ligand structure. For the $[Ag(L)]^+$ adduct (*m*/*z* 334.9), the species for L = 2,2′-DCPA (**2**) is clearly the most abundant. This point, coupled with the fact that the abundances of higher aggregates involving 2,2′-DCPA (i.e., those at *m*/*z* 592.9 and 821.2) are far lower than for $[Ag(\mathbf{2})]^+$, again suggests chelation of 2,2′-DCPA to silver(I).

Inspection of Figure 13 reveals that aggregates involving two silver(I) ions, namely $[Ag_2(L)(CF_3SO_3)]^+$ at *m*/*z* 592.9 and $[Ag_2(L)_2(CF_3SO_3)]^+$ at *m*/*z* 821.2, are most abundant for L = 2,3′-DCPA (**1**). It is proposed that this reflects the formation of cyclic dimers with 2,3′-DCPA in solution that are similar to those observed in complexes **4**−**6**.[10] Also, it is noted that the abundance of the $[Ag(\mathbf{L})]^+$ aggregate is low for L = 2,4′-DCPA (**3**). It is believed that this is due to the inability of 2,4′-DCPA to chelate to a single silver(I) ion as a result of the *para*-nitrile group. Further, higher aggregates with 2,4′-DCPA are present in relatively low abundance. This observation is most likely a result of the inability of 2,4′-DCPA to form cyclic dimers. It should be noted that a plot similar to that in Figure 13 was prepared from the acetone data and similar trends were observed in comparing aggregation behavior as a function of ligand structure (Figure 15 in the Supporting Information). Therefore, from the ESI-MS data presented here, it is believed that there is a preference for the formation of aggregates that maximize the coordination number of silver(I). As a result, chelated or cyclic aggregates should form where possible as opposed to open chain adducts which would contain terminal silver(I) ions.

In the discussion of the crystal structure of $[Ag(\mathbf{2})(CF_3SO_3)]$ (**7**) above, it was noted that 2,2′-DCPA coordinates to silver(I) in a *transoid* conformation to form the "half-bow-tie" chain topology (Figure 4). Why are chelated aggregates that are proposed to exist in solution not observed in the solid state? It is likely that chelated adducts are not observed in the solid state due to the inability of these aggregates to pack efficiently or to form a critical size nucleus. Further, crystallization of an adduct in which two molecules of 2,2′-DCPA chelate to a tetrahedral silver(I) ion would not allow coordination of the triflate ion which is observed in complexes **4**, **7**, and **8** presented here and other structures we have published previously.[11] Nonetheless, the presence of chelated aggregates as suggested by ESI-MS must perturb the equilibrium and may impact the formation of critical size nuclei prior to crystallization.

Conclusions

Aggregation of 2,2′-, 2,3′-, and 2,4′-dicyanodiphenylacetylene (2,2′, 2,3′-, and 2,4′-DCPA) with silver(I) salts has been investigated in the solid state by single-crystal X-ray diffraction and in solution by electrospray ionization mass spectrometry (ESI-MS). In the solid state, topology is found to depend on the substitution pattern of the ditopic ligand. With 2,3′-DCPA, cyclic dimers form with $AgCF_3SO_3$, $AgClO_4 \cdot H_2O$, and $AgSbF_6$. Significant deformations of the cyclic framework are observed as a function of the counterion. Crystallization of 2,2′-DCPA with $AgCF_3SO_3$ yields an infinite chain structure with a "half-bow-tie" motif as a result of the kinked nature of the ditopic ligand. With 2,4′-DCPA and $AgCF_3SO_3$, an infinite, undulating sheet is obtained in which helices of 2,4′-DCPA coordinated to silver(I) ions are bridged by triflate. Positive ion ESI-MS in acetone or acetonitrile provides evidence for solution aggregation of the ditopic ligands and silver(I) salts. This study is the first in which ESI-MS has been applied to systems that yield infinite coordination networks. The aggregation behavior is most strongly dependent on the structure of the ligand and the solvent employed and to a lesser degree on the counterion. For all of the systems investigated, aggregation of the ditopic ligands and silver(I) salts is significantly disrupted in acetonitrile at concentrations of approximately 10^{-3} M. Comparison of ESI-MS data for solutions of 2,2′-, 2,3′-, or 2,4′-DCPA and silver(I) salts in both acetone and acetonitrile shows that the dimers $[Ag_2(L)_2(X)]^+$ are most abundant for L = 2,3′-DCPA and X = $CF_3SO_3^-$, ClO_4^-, or SbF_6^-. It is believed that this reflects formation of cyclic dimers in solution similar to those characterized in the solid state. For solutions of 2,2′-DCPA and $AgCF_3SO_3$ in acetone or acetonitrile, aggregates of 2,2′-DCPA containing a single silver(I) ion dominate significantly over higher adducts. On the basis of this observation and molecular modeling, it is proposed that in solution 2,2′-DCPA chelates to a silver(I) ion. From the results presented here, it is believed that systematic studies of solution aggregation by ESI-MS will yield important information regarding nucleation prior to crystallization such that the process of self-assembly may be better understood.

(10) It should also be noted that, at millimolar concentrations in acetone and acetonitrile, the relative abundances of the dimers $[Ag_2(\mathbf{1})_2(ClO_4)]^+$ and $[Ag_2(\mathbf{1})_2(SbF_6)]^+$ are greater than those of $[Ag_2(\mathbf{2})_2(CF_3SO_3)]^+$ and $[Ag_2(\mathbf{3})_2(CF_3SO_3)]^+$. This suggests the formation of cyclic dimers in solution with 2,3′-DCPA and all three silver(I) salts.

(11) See refs 1c, 1d, and 6a and the following: (a) Hirsch, K. A.; Venkataraman, D.; Wilson, S. R.; Moore, J. S.; Lee, S. *J. Chem. Soc., Chem. Commun.* **1995**, 2199−2200. (b) Venkataraman, D.; Lee, S.; Moore, J. S.; Zhang, P.; Hirsch, K. A.; Gardner, G. B.; Covey, A. C.; Prentice, C. L. *Chem. Mater.* **1996**, *8*, 2030−2040.

Experimental Section

General Methods. Unless otherwise indicated, all starting materials were obtained from commercial suppliers (Aldrich, J. T. Baker, Eastman, EM Science, Fischer, Johnson-Matthey, Lancaster, and Mallinckrodt) and were used without further purification. Dichloromethane, ethyl acetate, and hexane were distilled prior to use. (Trimethylsilyl)acetylene (Farchan) was dried over anhydrous $MgSO_4$ and collected via vacuum transfer prior to use. Silver(I) triflate and silver(I) hexafluoroantimonate were stored in a desiccator with Drierite as the drying agent. Silver(I) perchlorate hydrate was stored in a refrigerator at 3 °C. All atmosphere-sensitive reactions were conducted under nitrogen using a Schlenk vacuum line. No precautions were taken to exclude water or air during crystallization experiments or during preparation of samples for ESI-MS. Analytical thin-layer chromatography (TLC) was performed on KIESELGEL F-254 precoated silica gel plates. Visualization was accomplished with a UV light. Flash chromatography was carried out with Silica Gel 60 (230−400 mesh) from EM Science.

^{1}H and ^{13}C NMR spectra were recorded on a Varian Unity 400 spectrometer. Chemical shifts were recorded in parts per million (δ), and splitting patterns were designated as s (singlet) or m (multiplet). Chloroform (δ 7.26 for ^{1}H, δ 77.0 for ^{13}C) was used as an internal standard for chloroform-*d*. Gas chromatography (GC) was performed on a Hewlett-Packard HP-5890 Series II gas chromatograph equipped with a 12.5 m × 0.2 m × 0.5 μm HP-1 methyl silicone column and fitted with a flame ionization detector using helium carrier gas at 30 mL/min. Low-resolution electron impact mass spectra were obtained using a Hewlett-Packard 5890 gas chromatograph combined with a 5970 Series mass-selective detector equipped with a 30 m HP-1 capillary column operating at 70 eV. High-resolution electron impact mass spectra were obtained on a Finnigan-MAT 731 spectrometer operating at 70 eV. Elemental analyses were performed by the University of Illinois Microanalytical Service Laboratory by combustion analysis on a Leeman Labs, Inc., Model CE440 Elemental Analyzer.

Crystallization with silver(I) triflate and silver(I) hexafluoroantimonate was accomplished by heating and slow cooling in a programmable oven equipped with a Thermolyne temperature controller. All crystals were stored in the dark until the collection of X-ray data. For X-ray analysis, all crystals were mounted using Paratone-N oil (Exxon).

X-ray data were collected on a Siemens SMART system equipped with a CCD detector at −75 °C using Mo Kα (λ = 0.710 73 Å) as the incident radiation. The intensity data were reduced by profile analysis and corrected for Lorentz, polarization, and absorption effects. Cell parameters and atomic coordinates were tested for higher symmetry using the PLATON program.[12] Structure solutions were obtained by direct methods and were refined using full-matrix least-squares on all reflections, based on F_o^2, with SHELXTL.[13]

Solutions for electrospray ionization mass spectrometry (ESI-MS) were prepared using reagent grade acetone or acetonitrile. Vials were lined with Teflon film prior to sealing them with a screw cap. ESI-MS was performed on a Fisons Instruments VG QUATTRO spectrometer. For the ESI-MS data, masses and intensities were compared to those calculated using the Isotope Pattern Calculator program (ver. 1.6.5, Macintosh).[14]

CAUTION: One of the crystallization procedures involves $AgClO_4 \cdot xH_2O$ ($x \sim 1$), which is an oxidizer.

2-[(Trimethylsilyl)ethynyl]benzonitrile (9). 2-Bromobenzonitrile (5.01 g, 27.52 mmol), $Pd(dba)_2$ (0.32 g, 0.56 mmol), CuI (0.11 g, 0.58 mmol), and Ph_3P (0.72 g, 2.75 mmol) were combined with triethylamine (100 mL) in a dry, heavy-walled tube sealed with a Teflon screw cap. The resulting mixture was degassed and back-filled with nitrogen three times and left under nitrogen at room temperature. Dry (trimethylsilyl)-acetylene (6.0 mL, 42.46 mmol) was then added via syringe. The tube was sealed with the Teflon screw cap and placed in an oil bath. Heating at 75 °C for 21 h produced an orange solution with a precipitate which was presumed to be triethylammonium bromide. The mixture was cooled to room temperature and diluted with CH_2Cl_2 (100 mL). The resulting solution was concentrated in vacuo to yield crude product as a dark red liquid with black and green solids. Column chromatography (15/1 hexane/ethyl acetate (v:v)) afforded **9** as a yellow liquid (4.39 g, 80% yield, 97% pure by GC): R_f 0.36 (15/1 hexane/ethyl acetate); ^{1}H NMR (400 MHz, $CDCl_3$) δ 7.62 (m, 1H), 7.53 (m, 2H), 7.39 (m, 1H), 0.29 (s, 9H); ^{13}C NMR (100 MHz, $CDCl_3$) δ 132.5, 132.4, 132.2, 128.4, 126.9, 117.3, 115.7, 102.1, 100.5, −0.4; LRMS (EI) *m*/*z* 199 (7), 185 (17), 184 (100), 154 (14); HRMS (EI) calcd for $C_{12}H_{13}NSi^+$ 199.0817, found 199.0823.

2,3′-Dicyanodiphenylacetylene (1). To a solution of 2-[(trimethylsilyl)ethynyl]benzonitrile (**9**; 4.15 g, 20.82 mmol) in CH_2Cl_2 (15 mL) and MeOH (30 mL) was added a trace of K_2CO_3. The brown mixture was degassed and back-filled with nitrogen three times and stirred under nitrogen at room temperature for 55 min, resulting in a yellow mixture. The conversion of **9** to 2-ethynylbenzonitrile was confirmed by GC and GC/MS (LRMS (EI) showed the desired molecular ion of *m*/*z* 127 for $C_9H_5N^+$). The terminal acetylene was not isolated. Next, in a dry, heavy-walled tube sealed with a Teflon screw cap were placed 3-bromobenzonitrile (2.32 g, 12.72 mmol), $Pd(dba)_2$ (0.13 g, 0.22 mmol), CuI (0.05 g, 0.26 mmol), Ph_3P (0.31 g, 1.18 mmol), and triethylamine (50 mL). This mixture was degassed and back-filled with nitrogen three times and left under nitrogen at room temperature. A portion of the CH_2Cl_2/MeOH solution of 2-ethynylbenzonitrile (22 mL, 1.29 g (10.15 mmol) of 2-ethynylbenzonitrile assuming quantitative conversion from **9**) was then added via syringe. The tube was sealed with the Teflon screw cap and placed in an oil bath. Heating at 77 °C for 21 h produced a brown solution with a precipitate which was presumed to be triethylammonium bromide. This mixture was cooled to room temperature, dissolved in CH_2Cl_2 (100 mL), and concentrated in vacuo to yield crude product as a brown solid. Column chromatography (CH_2Cl_2) afforded **1** as a yellow solid. Recrystallization from 1/1 benzene/hexane (v:v) afforded pure **1** as a white solid (1.42 g, 61% yield, 99% pure by GC): R_f 0.44 (CH_2Cl_2); ^{1}H NMR (400 MHz, $CDCl_3$) δ 7.86 (m, 1H), 7.82 (m, 1H), 7.70 (m, 1H), 7.63 (m, 3H), 7.49 (m, 2H); ^{13}C NMR (100 MHz, $CDCl_3$) δ 136.0, 135.0, 132.7, 132.5, 132.3, 132.2, 129.4, 129.0, 126.1, 123.6, 117.8, 117.3, 115.5, 113.0, 93.0, 87.6; LRMS (EI) *m*/*z* 229 (18), 228 (100), 227 (12), 201 (11); HRMS (EI) calcd for $C_{16}H_8N_2^+$ 228.0687, found 228.0687. Anal. Calcd for $C_{16}H_8N_2$: C, 84.19; H, 3.53; N, 12.28. Found: C, 83.80; H, 3.55; N, 12.17.

2,2′-Dicyanodiphenylacetylene (2). By following the procedure used to prepare 2,3′-dicyanodiphenylacetylene (**1**), 2-bromobenzonitrile (1.43 g, 7.86 mmol), $Pd(dba)_2$ (0.08 g, 0.14 mmol), CuI (0.03 g, 0.16 mmol), Ph_3P (0.19 g, 0.72 mmol), and triethylamine (30 mL) were combined in a dry, heavy-walled tube sealed with a Teflon screw cap. A solution of 2-ethynylbenzonitrile (0.89 g, 7.00 mmol (assuming quantitative conversion from trimethylsilyl-protected precursor **9**)) in CH_2Cl_2 (10 mL) and MeOH (20 mL) was added to the mixture via syringe. Heating at 80 °C for 20 h produced a brown solution with a precipitate which was presumed to be triethylammonium bromide. The mixture was cooled to room temperature, dissolved in CH_2Cl_2 (100 mL), and concentrated in vacuo to afford crude product as a brown solid. Column chromatography (4/1 CH_2Cl_2/hexane (v:v)) afforded **2** as a yellow solid. Recrystallization from 1/1 benzene/hexane (v:v) afforded pure **2** as a light yellow needles (0.95 g, 59% yield, 99% pure by GC): R_f 0.20 (4/1 CH_2Cl_2/hexane); ^{1}H NMR (400 MHz, $CDCl_3$) δ 7.75 (m, 2H), 7.70 (m, 2H), 7.61 (m, 2H), 7.48 (m, 2H); ^{13}C NMR (100 MHz, $CDCl_3$) δ 132.9, 132.7, 132.5, 129.2, 125.8, 117.2, 115.2, 91.2; LRMS (EI) *m*/*z* 229 (18), 228 (100), 227 (13), 201 (14); HRMS (EI) calcd for $C_{16}H_8N_2^+$ 228.0687, found 228.0687. Anal. Calcd for $C_{16}H_8N_2$: C, 84.19; H, 3.53; N, 12.28. Found: C, 84.26; H, 3.32; N, 12.28.

4-[(Trimethylsilyl)ethynyl]benzonitrile (10). By following the procedure used to prepare 2-[(trimethylsilyl)ethynyl]benzonitrile (**9**), 4-bromobenzonitrile (5.01 g, 27.52 mmol), $Pd(dba)_2$ (0.31 g, 0.54 mmol), CuI (0.10 g, 0.53 mmol), Ph_3P (0.72 g, 2.75 mmol), triethylamine (100 mL), and trimethylsilylacetylene (6.0 mL, 42.46 mmol) were combined in a dry, heavy-walled tube sealed with a Teflon screw cap. Heating for 16 h at 75 °C produced an orange solution with a

(12) Spek, A. L. *J. Appl. Crystallogr.* **1988**, *21*, 578−579.

(13) The SHELXTL X-ray structure refinement package consists of SAINT Version 4, SHELXTL Version 5, and SMART Version 4 and is marketed by Siemens Industrial Automation, Inc., Madison, WI.

(14) Isotope Pattern Calculator, Version 1.6.5: Arnold, L. University of Waikato, Hamilton, New Zealand, 1990.

precipitate which was presumed to be triethylammonium bromide. The mixture was cooled to room temperature, diluted with Et_2O (250 mL), and filtered to remove the precipitate. The yellow filtrate was concentrated in vacuo to yield crude product as a yellow solid. Column chromatography (18/1 hexane/ethyl acetate (v:v)) afforded **10** as a white solid (4.48 g, 81% yield, 98% pure by GC): R_f 0.36 (18/1 hexane/ethyl acetate); ^{1}H NMR (400 MHz, $CDCl_3$) δ 7.58 (m, 2H), 7.52 (m, 2H), 0.26 (s, 9H); ^{13}C NMR (100 MHz, $CDCl_3$) δ 132.4, 131.9, 127.9, 118.4, 111.7, 102.9, 99.5, −0.3; LRMS (EI) *m*/*z* 199 (24), 185 (18), 184 (100), 154 (6); HRMS (EI) calcd for $C_{12}H_{13}NSi^+$ 199.0817, found 199.0817. Anal. Calcd for $C_{12}H_{13}NSi$: C, 72.31; H, 6.57; N, 7.03. Found: C, 71.99; H, 6.63; N, 7.09.

4-Ethynylbenzonitrile (11). To a solution of 4-[(trimethylsilyl)-ethynyl]benzonitrile (**10**; 3.38 g, 16.96 mmol) in CH_2Cl_2 (30 mL) and MeOH (50 mL) was added a trace of K_2CO_3. The yellow solution was degassed and back-filled with nitrogen three times and stirred at room temperature under nitrogen. After 1.5 h, the solution was filtered to remove K_2CO_3 and the yellow filtrate was concentrated under reduced pressure to produce crude **11** as a tan solid. Purification by column chromatography (CH_2Cl_2) afforded **11** as a white solid (2.10 g, 97% yield, 99% pure by GC): R_f 0.67 (CH_2Cl_2); ^{1}H NMR (400 MHz, $CDCl_3$) δ 7.62 (m, 2H), 7.56 (m, 2H), 3.30 (s, 1H); ^{13}C NMR (100 MHz, $CDCl_3$) δ 132.6, 132.0, 126.9, 118.2, 112.2, 81.8, 81.5; LRMS (EI) *m*/*z* 128 (10), 127 (100), 100 (22), 99 (7), 76 (10), 74 (14); HRMS (EI) calcd for $C_{12}H_{13}NSi^+$ 127.0422, found 127.0422.

2,4′-Dicyanodiphenylacetylene (3). 2-Bromobenzonitrile (1.19 g, 6.54 mmol), 4-ethynylbenzonitrile (**11**; 0.75 g, 5.90 mmol), $Pd(dba)_2$ (0.07 g, 0.12 mmol), CuI (0.02 g, 0.11 mmol), and Ph_3P (0.16 g, 0.61 mmol) were combined with triethylamine (30 mL) in a dry, heavy-walled tube sealed with a Teflon screw cap. The resulting mixture was degassed and back-filled with nitrogen three times and heated under nitrogen at 75 °C for 24 h. An orange solution with a precipitate, presumably triethylammonium bromide, was obtained. The mixture was then cooled to room temperature and diluted with CH_2Cl_2 (100 mL). The resulting solution was concentrated in vacuo to yield crude product as a brown solid. Column chromatography (CH_2Cl_2) afforded **3** as a yellow solid. Recrystallization from 1/1 benzene/hexane (v:v) afforded pure **3** as a white solid in two crops (0.95 g (combined crops), 70% yield, 98% pure by GC): R_f 0.37 (CH_2Cl_2); ^{1}H NMR (400 MHz, $CDCl_3$) δ 7.72−7.59 (m, 7H), 7.48 (m, 1H); ^{13}C NMR (100 MHz, $CDCl_3$) δ 132.7, 132.4, 132.3, 132.2, 132.0, 129.0, 126.7, 126.0, 118.2, 117.2, 115.5, 112.4, 93.6, 89.3; LRMS (EI) *m*/*z* 229 (17), 228 (100), 227 (12), 201 (13); HRMS (EI) calcd for $C_{16}H_8N_2^+$ 228.0687, found 228.0685. Anal. Calcd for $C_{16}H_8N_2$: C, 84.19; H, 3.53; N, 12.28. Found: C, 84.10; H, 3.30; N, 12.29.

[Ag(2,3′-DCPA)(CF_3SO_3)]$_2$ (4). A mixture of 2,3′-dicyanodiphenylacetylene (10 mg, 0.04 mmol) and silver(I) triflate (12 mg, 0.05 mmol) in toluene (6 mL) was prepared in a clean vial with a Teflon-lined screw cap and heated in a programmable oven. Heating from room temperature to 100 °C at 20 °C/h, holding at 100 °C for 2 h, and cooling to room temperature at 1.2 °C/h yielded a homogeneous solution. Allowing the vial to stand for 2 d at room temperature afforded material suitable for X-ray analysis as colorless prisms. Anal. Calcd for $C_{17}H_8N_2O_3F_3SAg$: C, 42.08; H, 1.66; N, 5.77. Found: C, 42.16; H, 1.82; N, 5.34.

[Ag(2,3′-DCPA)(ClO_4)]$_2$ (5). A solution of 2,3′-dicyanodiphenylacetylene (10 mg, 0.04 mmol) and silver(I) perchlorate hydrate ($AgClO_4 \cdot xH_2O$, $x \sim 1$; 10 mg, 0.05 mmol) in acetone (6 mL) was prepared in a clean vial with a Teflon-lined screw cap. Evaporation of acetone over 5 d produced a white precipitate and colorless columnar crystals of which one was characterized as complex **5**.

{**[Ag(2,3′-DCPA)(SbF_6)]**}$_2$ **(6).** A mixture of 2,3′-dicyanodiphenylacetylene (10 mg, 0.04 mmol) and silver(I) hexafluoroantimonate (17 mg, 0.05 mmol) in benzene (6 mL) was prepared in a clean vial with a Teflon-lined screw cap and heated in a programmable oven. Heating from room temperature to 100 °C at 20 °C/h, holding at 100 °C for 2 h, and cooling to room temperature at 1.2 °C/h yielded a white precipitate and small colorless plates of which one was characterized as complex **6**.

[Ag(2,2′-DCPA)(CF_3SO_3)] (7). A mixture of 2,2′-dicyanodiphenylacetylene (10 mg, 0.04 mmol) and silver(I) triflate (12 mg, 0.05 mmol) in xylenes (6 mL) was prepared in a clean vial with a Teflon-lined screw cap and heated in a programmable oven. Heating from room temperature to 100 °C at 20 °C/h, holding at 100 °C for 2 h, and cooling to room temperature at 1.2 °C/h yielded a cluster of colorless plates. A crystal suitable for X-ray diffraction was cut from this cluster. Anal. Calcd for $C_{17}H_8N_2O_3F_3SAg$: C, 42.08; H, 1.66; N, 5.77. Found: C, 42.05; H, 1.72; N, 5.43.

[Ag(2,4′-DCPA)(CF_3SO_3)] (8). A mixture of 2,4′-dicyanodiphenylacetylene (10 mg, 0.04 mmol) and silver(I) triflate (12 mg, 0.05 mmol) in toluene (4 mL) was prepared in a clean vial with a Teflon-lined screw cap and heated in a programmable oven. Heating from room temperature to 100 °C at 20 °C/h, holding at 100 °C for 2 h, and cooling to room temperature at 1.2 °C/h yielded colorless prisms suitable for X-ray analysis. Anal. Calcd for $C_{17}H_8N_2O_3F_3SAg$: C, 42.08; H, 1.66; N, 5.77. Found: C, 41.95; H, 1.66; N, 5.74.

Acknowledgment. We are grateful to Dr. Richard Milberg of the Mass Spectrometry Center at the University of Illinois for performing electrospray ionization experiments. We thank the School of Chemical Sciences Materials Chemistry Laboratory at Illinois for X-ray data collection. The QUATTRO mass spectrometer was purchased in part with a grant from the Division of Research Resources, National Institutes of Health (RR 07141). We acknowledge the National Science Foundation (Grant CHE-94-23121) and the U.S. Department of Energy through the Materials Research Laboratory at the University of Illinois at Urbana-Champaign (Grant DEFG02-96-ER45439) for financial support of this work.

Supporting Information Available: Tables of X-ray data for complexes **4**−**8** including atomic coordinates, displacement parameters, and bond lengths and angles; a 50% probability thermal ellipsoid plot for each complex; electrospray ionization mass spectra for 2,3′-DCPA with both $AgClO_4 \cdot H_2O$ and $AgSbF_6$ in acetone and acetonitrile at concentrations of $(1.5-1.6) \times 10^{-3}$ M, 2,3′-DCPA with $AgCF_3SO_3$, $AgClO_4 \cdot H_2O$, or $AgSbF_6$ in acetonitrile at concentrations of 1.5×10^{-2} M, and 2,4′-DCPA with $AgCF_3SO_3$ in acetonitrile at concentrations of $(1.5-1.6) \times 10^{-3}$ M; expanded spectra of the region $[Ag_2(\mathbf{1})_2(X)]^+$ (X = $CF_3SO_3^-$, ClO_4^-, or SbF_6^-) with calculated isotope distributions; and a plot comparing abundances of key aggregates of the three ligands and $AgCF_3SO_3$ in acetone (51 pages). See any current masthead page for ordering and Internet access instructions.

JA971135G